Applied Catalysis B: Environmental 144 (2014) 243–251

Contents lists available at ScienceDirect

Applied Catalysis B: Environmental

journal homepage: www.elsevier.com/locate/apcatb

Activation of carbon-supported platinum catalysts by sodium for the low-temperature water-gas shift reaction

Branko Zugic [a], David C. Bell [b], Maria Flytzani-Stephanopoulos [a,*]

[a] Department of Chemical and Biological Engineering, Tufts University, Medford, MA 02155, United States
[b] School of Engineering and Applied Sciences, Harvard University, Cambridge, MA 02138, United States

ARTICLE INFO

Article history:
Received 14 May 2013
Received in revised form 21 June 2013
Accepted 1 July 2013
Available online 11 July 2013

Keywords:
Pt catalysts
Carbon nanotubes
Alkali promotion
Water-gas shift reaction

ABSTRACT

The activation of multi-walled carbon nanotube-supported platinum catalysts for the low-temperature water-gas shift reaction is demonstrated by the addition of sodium. Nitric acid oxidation of the carbon nanotubes allows for the addition of sodium through ion-exchange and creates anchoring sites for platinum. We show that an oxidized platinum state is stabilized by the presence of sodium. Evidence for a sodium-promoted Pt-$(OH)_x$ active site is given through XPS analysis of the catalysts before and after reaction and confirmed by CO-TPR. Removal of the oxygen groups and partial removal of sodium by annealing the Na-modified carbon nanotubes to 800 °C in inert atmosphere creates a surface on which Pt is initially very active, but of lower stability due to the absence of a sufficient number of surface sodium anchoring sites.

1. Introduction

The water-gas shift reaction is an essential component of reformate fuel gas upgrading processes for hydrogen production and purification [1]. When used as a part of PEM fuel cell systems, the WGS catalyst must be particularly robust due to frequent startup–shutdown cycles and potential exposure to air. Due to the susceptibility of the industrial copper catalysts to deactivation under such conditions, interest in noble metals as potential replacements has grown in recent years and many catalyst formulations have been examined [2,3].

Platinum, in particular, has been heavily studied as an alternative to the copper-based water-gas shift catalyst. Typical catalyst formulations have included Pt/CeO_2 [4,5], Pt/TiO_2 [6,7], Pt/Al_2O_3 [8,9], and Pt/ZrO_2 [10]. The activity of such materials has been linked to the oxygen defect concentration of the metal oxide support [4,11–13] and its ability to stabilize platinum in its active (Pt-O_x) state [3,14,15]. As a result, significant research efforts have focused on understanding the interaction of Pt with ceria [16] and modified ceria [17] due to the high activity (and defect concentrations) of these catalysts. Despite their high performance, ceria-based catalysts are deactivated under frequent shutdown/restart operation [18] as a result of hydroxycarbonate formation [5] and the destabilization of the active Pt-O_x site. At high temperatures, sintering of the platinum metal and the ceria support is the main reason for deactivation [19]. Alternatives to ceria are thus actively investigated.

A new class of alkali-promoted platinum catalysts has recently emerged as an alternative to ceria-supported Pt. The addition of alkali has been shown to improve the activity of Pt on a variety of oxide supports including ZrO_2 [20,21], CeO_2 [22,23], TiO_2 [24], and Al_2O_3 [25,26]. In the presence of alkali, Pt can be used most efficiently even on an inert support like silica, as has been demonstrated by Flytzani-Stephanopoulos and co-workers [25,27].

The latter work has presented evidence that a similar mechanism to that observed on Pt/CeO_2 is also plausible for these catalysts, whereby oxygen is supplied to the active site in the form of hydroxyls, via sodium (or potassium) atoms, bound to Pt with oxygen links in a Pt-Na(K)-$O_x(OH)_y$ cluster [25]. Water can easily be dissociated on these clusters and the CO reaction with —OH is catalyzed at low temperatures. Indeed, the apparent WGS activation energies of Pt on any oxide support are similar (~70 kJ/mol) [4,8,24,25,28], supporting the notion of a common Pt-$(OH)_x$ site. It was also recently shown that alkali addition to encapsulated Pt@SiO_2 catalysts promotes their WGS activity and provides structural stability to platinum which allows for stable activity in cyclic operation [27].

To further probe the need for a metal oxide as a carrier for active platinum catalysts, we have examined carbon supports, on which platinum is typically inactive for the low-temperature WGS reaction. In this work, we demonstrate that we can activate platinum

* Corresponding author at: Tufts University, Department of Chemical and Biological Engineering, 4 Colby Street, Medford, MA 02155, United States.
Tel.: +1 617 627 3048.
E-mail addresses: stephanopoulos@tufts.edu, mflytzan@tufts.edu, apcatb@tufts.edu (M. Flytzani-Stephanopoulos).

0926-3373/$ – see front matter © 2013 Elsevier B.V. All rights reserved.
http://dx.doi.org/10.1016/j.apcatb.2013.07.013

on inert carbon surfaces by the addition of alkali promoters. The remarkable improvement in activity upon the addition of sodium is thought to be directly related to the state of platinum.

Previous studies on carbon-supported platinum catalysts have shown the stabilizing and promoting effect of calcium on activated carbon-supported platinum for carbon dioxide hydrogenation [29]. Additionally, surface oxygen groups on carbon supports have been shown to have significant influence on catalytic performance in selective hydrogenation reactions [30]. Further understanding the interplay between surface oxygen groups and alkali promoters may allow for improved and more economical platinum-based catalyst design for a number of applications, such as hydrogenation [30] and oxygen reduction reactions [31,32].

Here we use a multi-step process for the synthesis of sodium-promoted platinum catalysts supported on multi-walled carbon nanotubes (MWNTs). While simple co-impregnation of Pt and Na precursors suffices to create an active catalyst, the approach followed in this work allows for the identification of the important oxygen anchoring sites on carbon surfaces. This may also be useful for the design of other dispersed M-O_x species on carbons.

2. Experimental

2.1. Catalyst preparation

The preparation of the catalyst was performed in a step-wise manner using carbon-modification techniques similar to those described by Roman-Martinez et al. [29]. A schematic of the process employed is shown in Fig. 1. A detailed description of the preparation steps is given below.

MWNT oxidation. Multi-walled carbon nanotubes (>95%, OD 20–30 nm, length 10–30 μm) were purchased from Cheap Tubes, Inc. Introduction of surface oxygen was performed by nitric acid oxidation. The as-received MWNTs (denoted C_N) were suspended in 70% HNO_3 (Alfa Aesar) (25 mL per gram of MWNT) and refluxed at 120 °C for 2 h (denoted 2h-C_N). After refluxing, the oxidized MWNTs were filtered and washed repeatedly with deionized water until neutral pH. The washed nanotubes were placed in a vacuum oven and dried overnight at 60 °C.

Alkali-metal ion exchange and annealing. Introduction of sodium was performed by ion-exchange, following the method used by Roman-Martinez et al. [29]. The 2h-C_N were suspended in a 1 M sodium acetate solution (50 mL per gram 2h-C_N) and refluxed at 60 °C for 24 h. Following the ion-exchange, the MWNTs were filtered, washed repeatedly with deionized water, and dried in a vacuum oven overnight at 60 °C. These materials are labeled Na-2h-C_N.

The heat-treatment of 2h-C_N and Na-2h-C_N supports was performed at 800 °C under flowing helium in a quartz packed bed reactor in order to decompose surface oxygen groups. The supports were maintained at 800 °C for 2–4 h.

Platinum deposition. Platinum was deposited on the MWNT supports by incipient wetness impregnation. Briefly, to prepare 1 g of 1 wt% Pt catalyst, 0.02 g tetraamine platinum nitrate (Alfa Aesar) was dissolved in 1.5 mL (i.e. pore volume of all supports = 1.5 mL/g) deionized water. The platinum solution was added drop-wise to the support, ensuring even distribution of the solution, until a dry paste was formed. The impregnated support was dried in a vacuum oven overnight at 60 °C. The dried samples were crushed and stored in glass vials until reaction (all catalysts were heated in He to 400 °C at a rate of 10 °C/min and held at temperature for 1 h prior to use).

2.2. Characterization

High-resolution transmission electron microscopy (HRTEM) was performed using a JEOL 2100 at an operating voltage of 200 kV. Aberration-corrected HAADF-STEM imaging was performed using a Zeiss Libra 200 MC microscope operated at 200 kV. TEM samples were prepared by dispersing the powdered samples in ethanol and dropping onto a 200 mesh copper grid coated with a lacey carbon film. Particle sizes were estimated from the images by counting at least 200 particles.

BET surface area measurements were carried out in a Micromeritics AutoChem 2920 II system. 0.1 g of catalyst was placed in a U-shaped reactor and purged in flowing helium at 110 °C prior to BET measurement.

He-TPD was performed in a Micromeritics AutoChem 2920 II by placing 0.1–0.2 g of sample in a U-shaped quartz tube between two plugs of quartz wool, purging in helium, and linearly heating the sample at a rate of 10 °C/min in flowing helium (30 mL/min) while monitoring the gas effluent with a residual gas analyzer (SRS RGA 200).

CO-TPR was performed in a Micromeritics AutoChem 2920 II instrument on a used catalyst (following an in situ temperature-programmed surface reaction test), followed by hydration using a water-saturated helium gas flow. After cooling to room temperature, the reactor was purged with a 10% CO—He gas and heated at a rate of 10 °C/min. Effluent gases were analyzed using a residual gas analyzer (SRS RGA 200).

X-ray photoelectron spectroscopy (XPS) studies were performed using a Thermo Scientific K-Alpha operated using Al K-alpha radiation and a pass energy of 20–40 eV.

X-ray diffraction (XRD) was performed on a PANalytical X'Pert Pro using Cu K-alpha radiation, equipped with high-speed Bragg-Brentano Optics.

2.3. Activity tests

Steady-state activity tests were performed using an in-house packed-bed quartz micro-reactor operated at atmospheric pressure. The feed and product gas compositions were analyzed using an SRI 331 gas chromatograph (GC) equipped with a Carbosphere 80/100 packed column and a TCD detector. In a typical experiment, 0.1–0.2 g of catalyst was diluted with calcined quartz sand and loaded between two plugs of quartz wool. The gas composition for typical product-free activity tests was 2% CO–10% H_2O–88% He, using a flow rate of 70 mL/min.

Temperature-programmed surface reaction (TPSR) tests were performed in a Micromeritics AutoChem 2920 II system. The catalyst (0.1 g) was placed in a U-shaped reactor between two plugs of quartz wool and treated in flowing helium to 400 °C. After cooling to room temperature, a water-saturated 10% CO—He gas was flowed to the reactor (30 mL/min). The temperature was ramped linearly at 10 °C/min to 400 °C and the gas effluent analyzed by a residual gas analyzer (SRS RGA 200).

3. Results and discussion

3.1. Support characterization

The MWNT support materials were characterized at various stages of treatment by XPS and TPD in order to identify changes at the surface. The elemental compositions of the MWNT surfaces, as determined by XPS after various treatments, are shown in Table 1. The nitric acid treatment (2h-C_N) significantly increases the amount of surface oxygen (3.2 at%) compared to as-received MWNT (1.6 at%). While longer acid treatment allows for higher surface oxygen content, it is also known to cause significant structural changes to the nanotubes (e.g. opening of tips), and was therefore avoided in this study. The ion-exchange of sodium (Na-2h-C_N) onto the 2-h acid-treated MWNT results in the introduction of 0.7 at% sodium at

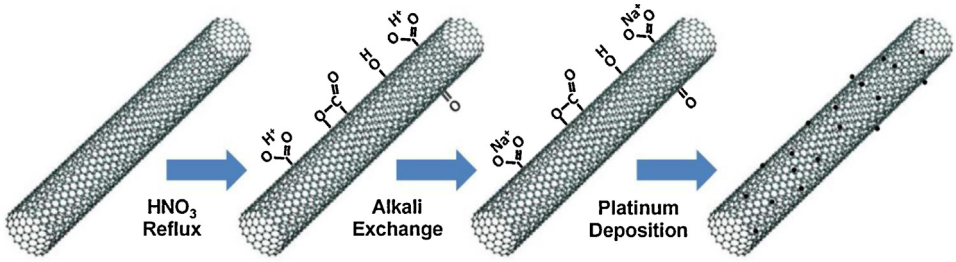

Fig. 1. Schematic of the preparation of alkali-promoted Pt/MWNT catalysts.

Table 1
Characterization of treated MWNT supports.

Support	Surf. concentration[a]			SA[b] (m^2/g)	He-TPD	
	C (at%)	O (at%)	Na (at%)		CO_2 (μmol/g)	CO (μmol/g)
C_N (as-received)	98.4	1.6[c]	0	180	–	–
2h-C_N	96.8	3.2	0	160	185	380
Na-2h-C_N	95.8	3.5	0.7	160	150	200
800-2h-C_N	99.5	0.5	0	150	–	–
800-Na-2h-C_N	98.7	1.0	0.3	160	–	–

[a] Determined by XPS.
[b] Determined by BET nitrogen desorption porosimetry.
[c] Oxygen content varied from batch to batch.

the surface and does not significantly increase the oxygen content. Furthermore, the BET surface area is found to change only slightly upon acid-treatment, indicating that the MWNT structure of the samples did not change significantly. The small decrease in surface area following HNO_3 treatment may suggest the removal of amorphous carbon that is sometimes present on the nanotube surface as a result of purification [33].

He-TPD experiments were performed on these materials in order to monitor the evolution of CO and CO_2, corresponding to the decomposition temperatures of various surface oxygen groups [34,35]. These results demonstrate that the as-received MWNTs (Fig. 2A) mainly contain groups that decompose at temperatures above 400 °C, indicating a high fraction of C=O (anhydride, phenol, lactone, quinone, and carbonyl) [34,36]. The acid-treated MWNTs (Fig. 2B) clearly exhibit a much higher degree of functionalization, spanning the range from oxygen groups of low stability (i.e. decomposing at <400 °C) that result in the production of CO_2, to those of higher stability (i.e. decomposing at >400 °C) that result in the production of CO. CO_2-producing groups are generally assigned to carboxylic acids (100–300 °C), anhydrides (400–600 °C) and lactones (600–800 °C) [34,37,38]. CO-producing groups, as previously mentioned, are assigned to anhydrides (400–600 °C), phenols (500–750 °C), and carbonyls and quinones (700–1000 °C) [34,38]. These are approximate assignments that are used here to interpret the relative importance of surface oxygen groups.

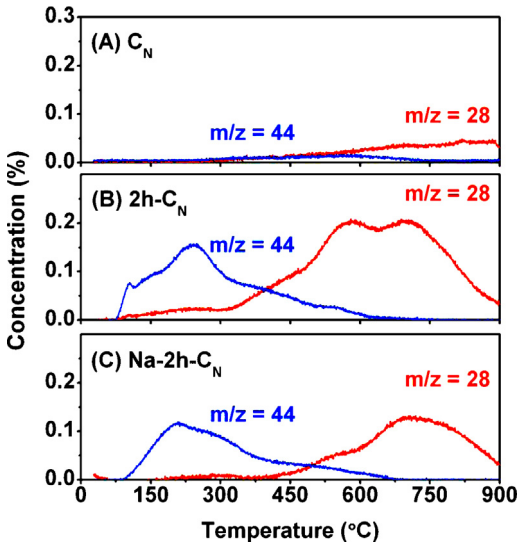

Fig. 2. Temperature-programmed desorption of CO and CO_2 from (A) as-received MWNT (B) acid treated MWNT and (C) Na-modified acid treated MWNT. Conditions: 30 mL/min He flow, 10 °C/min heating rate.

Upon sodium ion-exchange of the acid-treated MWNT, a significant change in the TPD profiles is observed (Fig. 2C). Namely, the CO_2 peaks at 120 °C and 210 °C as well as the CO peak at ~560 °C are apparently suppressed by the addition of alkali metal. These low-temperature CO_2 peaks are assigned to adsorbed carbon dioxide and carboxylic acid groups in various environments [38,39], while the higher-temperature CO peak (which is accompanied by a small CO_2 peak in the 2h-C_N sample that is also suppressed in the exchanged material) can be attributed to carboxylic anhydrides and phenols [34,38]. However, of these groups, only carboxylic acids are expected to be able to electrostatically stabilize sodium by ion-exchange [39], suggesting that the higher temperature peaks are likely due to the step-wise decomposition of the carboxylic groups (i.e. dehydration to carboxylic anhydrides followed by decomposition) [35,39]. Carbons that have been oxidized and ion-exchanged with calcium have been reported to retain the local chemistry around the alkaline earth ion upon heat treatment in inert gas [40], which may explain the apparent stabilization of oxygen on the surface of the MWNTs.

Based on the quantification of He-TPD measurements presented in Fig. 2 and Table 1, 250 μmol of oxygen (CO_2 + CO) per gram of support is stabilized on the surface by the addition of sodium. This corresponds to the difference between the XPS signals of 800-2h-C_N and 800-Na-2h-C_N in Table 1. Heat treatment of Na-2h-C_N to 800 °C (800-Na-2h-C_N) leaves 1 at% surface oxygen, compared to 0.5 at% for annealed 2h-C_N (i.e. 800-2h-C_N). The atomic ratio of the stabilized oxygen in the Na-exchanged sample (i.e. the difference of 800-Na-2h-C_N and 800-2h-C_N) to that of sodium is determined to be 3:2, indicating the presence of sodium carbonate.

Annealing the 2h-C_N support to 800 °C removes most of the surface oxygen, although a small amount (0.5 at%) remains. It has

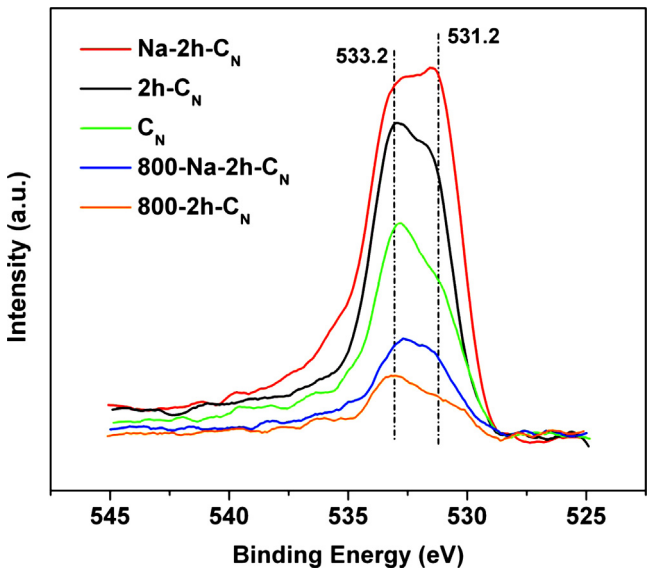

Fig. 3. O 1s XPS signals of as-received (C_N) and treated MWNT supports (2 h acid treatment, Na ion-exchange, and 800 °C heat treatment).

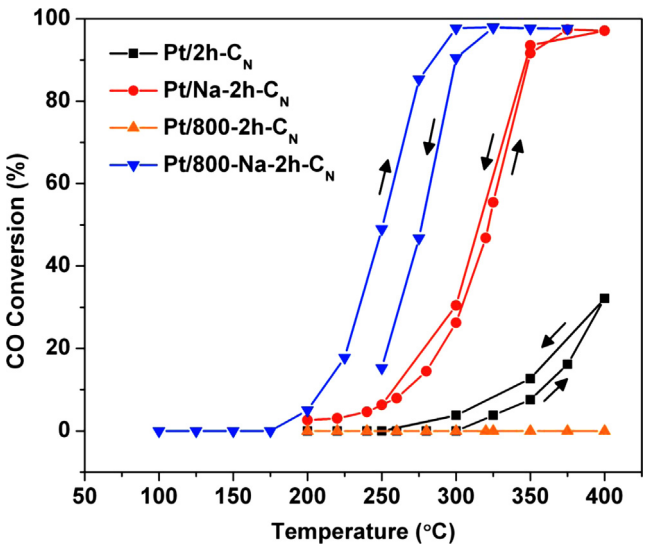

Fig. 4. WGS activity of Pt catalysts on acid-treated (Pt/2h-C_N and Pt/Na-2h-C_N) and annealed (Pt/800-2h-C_N and Pt/800-Na-2h-C_N) MWNT supports. Gas flow rate = 70 mL/min (2% CO–10% H_2O–He); 0.1 g catalyst.

been suggested that the remaining groups are stable basic groups (pyrone-like structures) [36,37] that are effective in preventing the sintering of active metals [41]. Sodium ion-exchange does not occur on these surfaces due to the absence of carboxylic acid groups. It is important to note that the exposure of Na-2h-C_N to the 800 °C treatment clearly results in an apparent loss of sodium, as shown in Table 1. This may be due to the removal of surface groups and the high vapor pressure of Na at this temperature. In fact, it has been shown that in the presence of carbon, sodium carbonate decomposition (to gas-phase Na and CO_2) is markedly enhanced, with decomposition beginning at 800 °C [42]. Due to the poor structure of the as-received MWNTs (see Fig. S1), migration of Na into the nanotubes may also occur, as is shown for platinum below.

The intercalation of sodium is unlikely due to its weak interaction with highly graphitic structures [43,44] and the low stability of intercalation compounds under the reaction conditions used here (i.e. exposure to air and high temperatures in the presence of water) [45]. Furthermore, powder X-ray diffraction analysis of these two annealed samples shows no shift in the (0 0 2) carbon peak in the presence of sodium (see Fig. S2). For intercalation compounds, the expansion of the intershell spacing due to the intercalation of alkali is typically manifested as a shift in this peak due to the swelling of the carbon structure [46].

The O 1s spectra of the various support materials are shown in Fig. 3 and corroborate the TPD findings above (C 1s spectra are shown in Fig. S3). The assignment of specific oxygen group contributions to the O 1s spectra of modified carbons varies substantially throughout the literature. We therefore use the general assignments here: C═O at 531.2 eV and C—O at 533.2 eV [36]. Adsorbed hydroxyl groups are have also been assigned around 531.2 eV [47] and carbonates at 531.9 eV [48].

The as-received MWNTs (C_N) have a significant amount of surface oxygen (1.6 at%) of C═O and C—O type, due to the presence of the high-stability oxygen groups previously mentioned (carbonyls, quinones, pyrone) [35,49]. Oxidation of the as-received nanotubes by nitric acid (2h-C_N) results in a roughly parallel increase in the signals at 531.2 eV and 533.2 eV, corresponding to an increase of mainly carboxylic as well as anhydride acid groups [35]. Treatment of the oxidized MWNT to 800 °C (800-2h-C_N) results in a decrease of all oxygen components, except the thermally stable groups mentioned previously.

The ion-exchange of sodium with 2h-C_N (Na-2h-C_N in Fig. 3) results in a marked increase of the O 1s signal at 531.9 eV, corresponding to (sodium) carbonate groups [48]. A slight increase in intensity at high binding energies (i.e. 535 eV) corresponds to adsorbed water and CO_2 due to the presence of alkali. Upon heating this sample to 800 °C, all of the oxygen signals are decreased significantly (800-Na-2h-C_N). Compared to the annealed, sodium-free support, however, the contributions at 531.9 eV and 531.2 eV (likely corresponding to carbonate and hydroxyl groups) are more pronounced and apparently related to the presence of sodium.

3.2. Catalyst activity and characterization

Platinum catalysts (1 wt%) were prepared from each of the treated supports described above and calcined at 400 °C in helium prior to reaction. The resulting CO conversions in a product-free reaction feed gas are shown in Fig. 4. The Pt/800-2h-C_N catalyst shows no WGS activity; this is attributed to the low concentration of sites for water activation on this material. The introduction of surface oxygen to the MWNT prior to Pt addition slightly improves the activity, as shown for the Pt/2h-C_N catalyst. The activation by surface oxidation is unexpected, as these groups are not thought to exhibit the redox-type behavior that has been observed on many metal oxides. In fact, reports of Pt catalysts supported on carbon nanofibers have indicated that the incremental removal of oxygen groups increases catalyst activity for cinnemaldehyde hydrogenation due to the altered interaction of reactant with the support surface [30]. Further investigations showed that the presence of oxygen groups on carbon nanotubes stabilizes platinum in its cationic state [50]. It is conceivable that the ability of these oxygen groups to adsorb water in the vicinity of such cationic Pt species is what gives rise to the observed WGS activity.

The addition of Na by ion-exchange to the oxidized nanotubes prior to Pt deposition results in a marked increase in WGS activity. Thus, we verify here the promotional effect of Na on carbon-supported Pt catalysts for the WGS reaction, which has previously been reported only on metal oxide supports [20,24–28,35,37]. The WGS activity is further increased by the removal of all but a few surface oxygen groups during the heat-treatment to 800 °C prior to Pt addition (Pt/800-Na-2h-C_N). Interestingly, the promotional effect is enhanced even with the observed loss of sodium at the surface after the high temperature treatment (Table 1). This

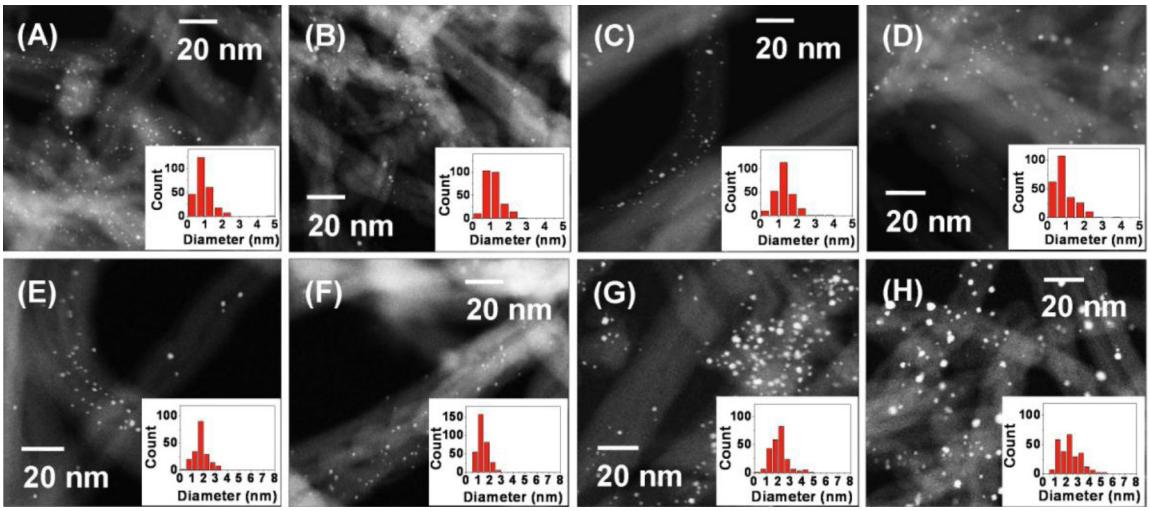

Fig. 5. Aberration-corrected HAADF-STEM images of freshly calcined (A) Pt/2h-C_N, (B) Pt/Na-2h-C_N, (C) Pt/800-2h-C_N, and (D) Pt/800-Na-2h-C_N, and used (E) Pt/2h-C_N, (F) Pt/Na-2h-C_N, (G) Pt/800-2h-C_N, and (H) Pt/800-Na-2h-C_N.

suggests that the number of active sites is increased when Pt is added to the annealed support (in the presence of Na) as very few oxygen anchoring sites are available on this material. Based on previous reports using carbon-supported Pt catalysts, it is also possible that surface oxygen groups present on the oxidized support negatively influence the activity as a result of interactions with adsorbates [30,51]. These groups are also known to promote the spillover of hydrogen and CO – particularly in the presence of water – and may influence the activity under the conditions used [52,53].

HAADF-STEM images of the catalysts before and after reaction are shown in Fig. 5. The average particle size of the annealed catalysts is generally observed to be higher due to the absence of surface oxygen groups that serve to anchor and disperse platinum. The as-calcined Pt/800-Na-2h-C_N sample, which gave the highest WGS activity (Fig. 4), was found to contain more than 50% of the platinum as sub-nm clusters and atoms (Fig. 5D). This finding is similar to that observed on silica-supported, Na-promoted Pt catalysts [25]. Fig. 6A clearly shows the presence of Pt atoms (circled regions) and the inter-planar spacing of the larger Pt particles, corresponding to the (1 1 1) crystal plane. Very few sub-nm species were present on the Na-free Pt/800-2h-C_N catalyst, shown in Fig. 5C and G. Given that the Pt/800-2h-C_N catalyst (employing carbon supports with no surface oxygen groups) is completely inactive for the WGS reaction, the promotional effect of sodium is thought to lie in its ability to activate water and to stabilize platinum in its active state, which is demonstrated below.

Following their use under WGS conditions, the particle size increases for all catalysts. However, as expected, the use of oxidized carbon supports results in the mildest agglomeration of platinum. The removal of these groups leads to more severe growth of platinum, yielding average particle sizes of 2.1–2.3 nm (Table 2), as well as resulting in the migration of Pt into the core of the MWNT due to the presence of poorly formed tubular structures in the as-received material (Fig. 6B). Interestingly, the particle size distribution of Pt/800-Na-2h-C_N following reaction (Fig. 5H) appears to be bimodal in nature; the local maximum at the higher particle size is similar to that observed on Pt/800-2h-C_N (Fig. 5G), while that at the lower particle size is centered at ~1 nm. This may be explained by the previously reported ability of sodium to stabilize platinum in its dispersed state [25,27], even in the absence of surface oxygen groups.

The characterization of the used catalysts by XPS and the average particle size determined from HAADF-STEM are shown in Table 2. The corresponding Pt 4f and O 1s signals (before reaction) are shown in Fig. 7. A loss of surface oxygen is observed for the Pt/2h-C_N catalyst compared to the parent support (2h-C_N in Table 1) after calcination in helium atmosphere due to the decomposition of surface oxygen groups. A further decrease is observed after

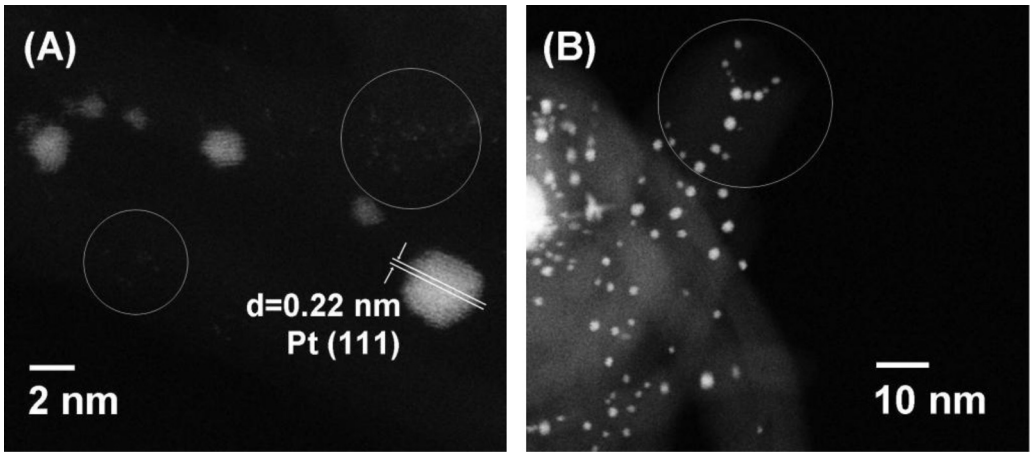

Fig. 6. Aberration-corrected HAADF-STEM images of (A) Pt/800-Na-2h-C_N after calcination at 400 °C in He and (B) Pt/800-2h-C_N after reaction conditions from the figure.

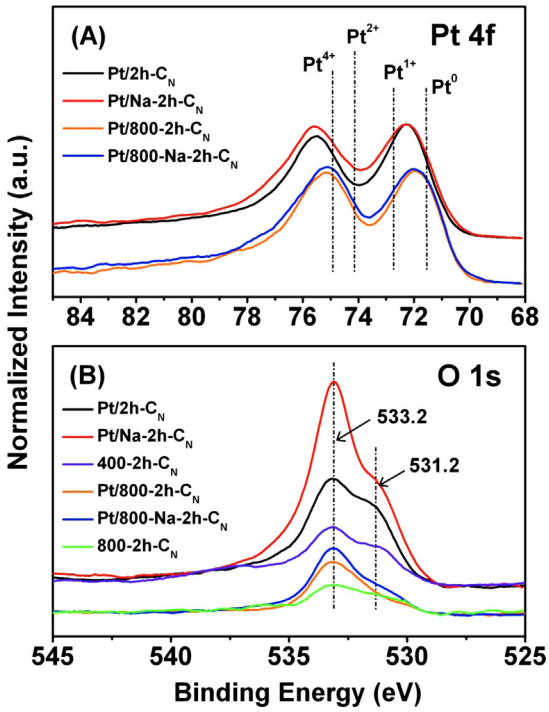

Fig. 7. (A) Pt 4f and (B) O 1s XPS signal of Pt catalysts calcined at 400 °C in flowing He. Pt $4f_{7/2}$ oxidation states of platinum are indicated on the plot.

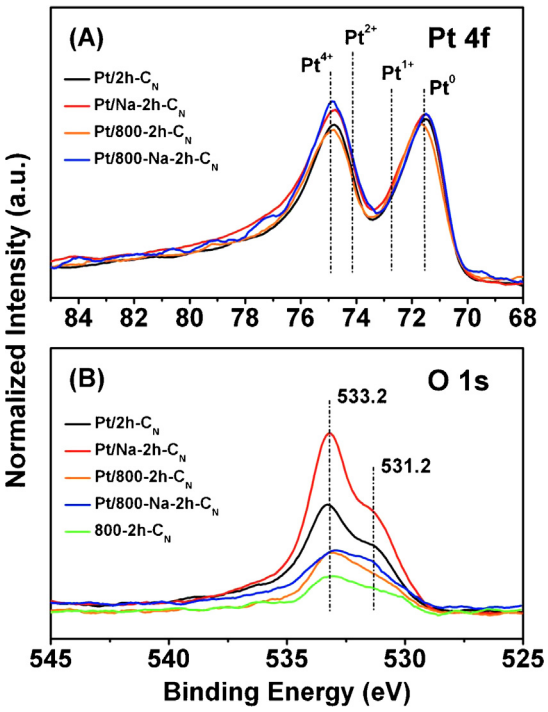

Fig. 8. (A) Pt 4f and (B) O 1s XPS signals of MWNT-supported platinum catalysts after the WGS activity tests in Fig. 4. Pt $4f_{7/2}$ oxidation states of platinum are indicated on the plot.

exposure to reaction conditions due to the reactivity of surface oxygen in the presence of CO. The fresh Pt/Na-2h-C_N, on the other hand, retains the same oxygen content as the parent support (Na-2h-C_N) after calcination. This is likely due to the aforementioned stability imparted by the presence of Na. However, a decrease in the oxygen content for this catalyst is also observed after exposure to reaction conditions. This indicates that not all of the oxygen groups on this material are necessary for activating and stabilizing Pt.

Conversely, the oxygen content of catalysts prepared on annealed supports is significantly lower. The marginal increase observed upon Pt addition and the subsequent decrease after exposure to reaction conditions likely reflects the oxygen associated with Pt, indicative of its oxidation state as shown in Figs. 7 and 8. The consistently higher oxygen content of the Na-promoted catalyst, however, demonstrates the ability of sodium to stabilize oxygen (and possibly activate water) on the surface. This oxygen is shown below to have an apparent influence on the state of Pt. The ~40% decrease in surface Pt concentration observed on these catalysts (compared to the oxygen-rich MWNT catalysts) is due to the propensity of Pt to be occluded inside the MWNT in the absence of surface anchoring sites, as shown in Fig. 6B, in addition to the growth of Pt particles over the course of reaction.

The Pt 4f and O 1s XP spectra of the fresh catalysts are shown in Fig. 7 and those of the used catalysts are shown in Fig. 8. These results reveal a direct effect of the alkali metal on the state of Pt. The Pt 4f spectrum indicates that a mixture of Pt^0 (71.4 eV) and Pt^{1+} (72.5 eV) [54] is generally observed after calcination in helium, as indicated by the average peak positions in Fig. 7A. The increase in intensity at the Pt^{2+} binding energy for Pt/Na-2h-C_N as compared to Pt/2h-C_N indicates that the addition of Na results in an apparent oxidation of Pt. This effect is somewhat dampened on the Pt/800-Na-2h-C_N due to the low concentration of Pt as a result of occlusion, however it can still observed in Fig. 7A as an increase in the intensity of the Pt $4f_{7/2}$ signal at ~74 eV and ~77 eV. Similar observations have been reported for alkali-promoted Pt/SiO_2 catalysts [25]. Furthermore, the higher average binding energy of the Pt $4f_{7/2}$ peak positions on oxygen-rich supports, as well as the absence of an

Table 2
Characterization of MWNT-supported Pt catalysts.

Catalyst	Concentration (at%)				Pt size[b] (nm)
	C	O	Pt	Na	
Pt/2h-C_N					
Calcined	97.8	2.1	0.07	0	0.9
Used[a]	98.0	1.9	0.07	0	1.7
Pt/Na-2h-C_N					
Calcined	95.8	3.5	0.07	0.6	1.1
Used[a]	97.2	2.2	0.06	0.5	1.4
Pt/800-2h-C_N					
Calcined	99.0	1.0	0.04	0	1.3
Used[a]	99.2	0.8	0.04	0	2.1
Pt/800-Na-2h-C_N					
Calcined	98.4	1.4	0.04	0.2	0.9
Used[a]	98.9	1.0	0.04	0.1	2.3

[a] Used catalysts analyzed after testing in 2%CO–10%H_2O–88%He at 200–400 °C.
[b] Determined from HAADF-STEM images.

apparent decrease in Pt concentration (Table 2), demonstrates the ability of surface oxygen groups to anchor platinum on the surface in its dispersed (i.e. Pt-O_{ad}) state [50,55–57].

Fig. 7B shows that an increase in O 1s intensity at 533.2 eV and 531.2 eV is observed for the Na-containing samples. For comparison, the O 1s spectra of the oxidized supports treated to 400 °C (400-2h-C_N) and 800 °C (800-2h-C_N) are also included. This comparison highlights that the contributions presented here are due to the introduction of Pt and Na, rather than oxygen groups remaining on the surface after helium treatment. The oxygen signals of the Pt/2h-C_N and Pt/Na-2h-C_N catalysts are difficult to interpret unambiguously due to the presence of a large number of surface oxygen groups. For Pt/800-Na-2h-C_N, however, the contribution at 533.2 eV may indicate the presence of a "bridging"-type oxygen [58,59] which can be attributed to a Pt-O-Na-type interaction, while that at 531.2 eV can be assigned to the presence of hydroxyls [47].

Fig. 8 shows the Pt 4f and O 1s signals of the catalysts after exposure to reaction conditions (Fig. 4). From Fig. 8A, it is clear that much of the platinum has been reduced to its metallic state in all materials. The predominance of larger Pt nanoparticles on the used catalysts in Fig. 5 is in line with this finding. Similarly to the Pt 4f analysis of the fresh catalysts, an increased Pt^{2+} contribution is clearly seen in Fig. 8A for the Na-promoted Pt after WGS reaction. The relative distribution of states obtained by the deconvolution of these spectra is listed in Table 3 (see Fig. S4 for deconvolution) and emphasizes this higher proportion of Pt^{2+} for Pt/Na-2h-C_N and Pt/800-Na-2h-C_N; the total Pt^{2+} (at%) calculated based on the surface Pt concentration is observed to be an order of magnitude greater for the Na-promoted samples. This indicates that the presence of sodium imparts an oxidative influence on specific Pt sites. Furthermore, stabilization of the individual Pt atoms and clusters is also observed on Pt/800-Na-2h-C_N (Fig. 6A). It is these finely dispersed, oxidized species that are key for the WGS activity. The observed drop in CO conversion after the WGS reaction at high temperature (Fig. 4) is attributed to a decrease in the number of these sites on the Pt/800-Na-2h-C_N catalyst. On the other hand, these sites are stable on the Pt/Na-2h-C_N catalyst, although fewer in number due to the limited interaction of Pt with the ion exchanged sodium sites (and strong interactions with other un-promoted surface oxygen groups). These findings point to the possibility of increasing the activity through preparation approaches that would maximize the platinum and sodium interaction.

The O 1s signals of the used catalysts indicate that the main contributions are centered at 531.2 eV and 533.2 eV. For the catalysts prepared on annealed supports (Pt/800-2h-C_N and Pt/800-Na-2h-C_N), the changes in the O 1s signal can be resolved more subtly, and a direct effect on the Pt/Na chemistry can be deduced. The O 1s signal of the 800-2h-M support, included in Fig. 8B for reference, represents oxygen remaining on the support (Table 1) following the 800 °C treatment in helium in the absence of Na. The corresponding Pt catalyst (Pt/800-2h-C_N) shows an increase in the observed amount of oxygen, which is stable on the surface both before and after reaction (Table 2). The increase in O 1s intensity is observed predominantly at 533.2 eV. Conversely, for the Na-containing Pt/800-Na-2h-C_N catalyst, the O 1s intensity at ~533 eV (due to the presence of Pt) is unchanged while the intensity at 531.2 eV is clearly increased. Previous studies on the oxidation of platinum surfaces have shown that Pt-OH interactions result in O 1s binding energies of ~531 eV, while Pt-H_2O and Pt-O species are seen at ~533 eV and ~530 eV, respectively [60–62]. We can conclude from these observations that the introduction of sodium into the Pt/C_N catalyst surface increases the hydroxyl content, and this stabilized hydroxyl interacts with (i.e. stabilizes) platinum clusters to promote the WGS reaction. In the absence of sodium, such activation of water in the proximity of platinum is not observed, as shown by the absence of an OH contribution at 531.2 eV.

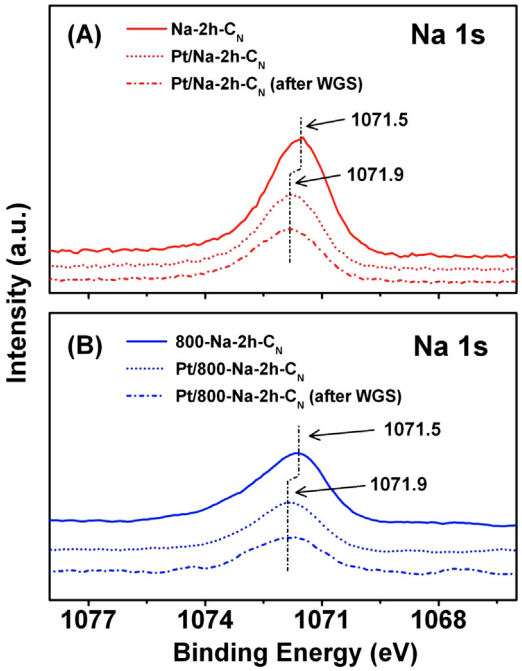

Fig. 9. Na 1s XPS signal of sodium-containing supports (A) with (Na-2h-C_N) and (B) without (800-Na-2h-C_N) surface oxygen (solid lines) and the corresponding platinum catalysts after calcination in flowing helium (dotted lines), and after WGS activity test from Fig. 4 (dash-dotted lines).

Fig. 9 shows the changes in the Na 1s signal for the sodium-containing supports and catalysts. Changes in sodium state upon the introduction of platinum corroborate the assertion that there is indeed an oxygen-mediated interaction with platinum. On the bare support materials, the peak is somewhat asymmetric and centered at 1071.5 eV, indicative of a sodium carbonate chemistry [63]. It is important to note that even upon heat treatment of the Na-2h-C_N (bare supports in Fig. 9A and B) to 800 °C in order to decompose the surface oxygen, the carbonate chemistry is retained. Upon the introduction of platinum and calcination to 400 °C, a shift to higher binding energy (1071.9 eV) is observed. This binding energy has previously been attributed to a partially oxidized sodium (NaO_x) structure [64]. Additionally, it excludes the possibility that sodium intercalation has taken place (Na 1s at ~1073 eV) [65]. It is conceivable that a Pt-Na-OH_x structure would result in an apparent partial oxidation of the sodium and a Na 1s binding energy somewhere between the initial carbonate state (1071.5 eV) and the fully oxidized sodium state (Na_2O at 1072.5 eV) [63]. This structure is apparently stable and is shown here to persist on both oxygenated and annealed MWNT-supported catalysts even after the WGS reaction.

We further confirm the assertion of activated hydroxyl species by performing CO-TPR experiments on the Pt/800-Na-2h-C_N catalyst. The sample was first subjected to a TPSR-mode WGS light off test to confirm its activity and stability over the course of up to four cycles. The CO-TPR was then performed on a pre-hydrated sample (using a H_2O-saturated helium flow). The evolution of H_2 and CO_2, corresponding to the WGS activity, is shown in Fig. 10. A deconvolution of the CO_2 signal shows a distinct peak, corresponding accurately to the observed hydrogen evolution. The CO_2/H_2 ratio of the integrated peaks was found to be 2, reflecting the stoichiometry of the WGS reaction (and an initially hydroxylated surface).

Based on the WGS results in Fig. 4, it is apparent that the initial activity of Pt/800-Na-2h-C_N is not retained over the course of the reaction conditions used. This can be understood in terms of the decreased number of anchoring sites (i.e. oxygen containing

Table 3
Relative distribution of Pt oxidation states in used catalysts.[a]

Catalyst	Fraction[b]			Total
	Pt^0	Pt^{1+}	Pt^{2+}	Pt^{2+} (at%)
Pt/2h-C_N	0.4	0.5	0.1	0.007
Pt/Na-2h-C_N	0.4	0.4	0.2	0.014
Pt/800-2h-C_N	0.5	0.4	0.1	0.004
Pt/800-Na-2h-C_N	0.5	0.2	0.3	0.012

[a] Used catalysts analyzed after testing in 2%CO–10%H_2O–88%He at 200–400 °C as in Fig. 4.
[b] Based on the deconvolution of the Pt 4f spectra shown in Fig. 8A; using Pt $4f_{7/2}$ B.E. values (FWHM in parentheses) Pt^0 = 71.4 eV (1.2), Pt^{1+} = 72.5 eV (1.5), Pt^{2+} = 74.1 eV (1.6), Pt^{4+} = 74.9 eV (N/A).

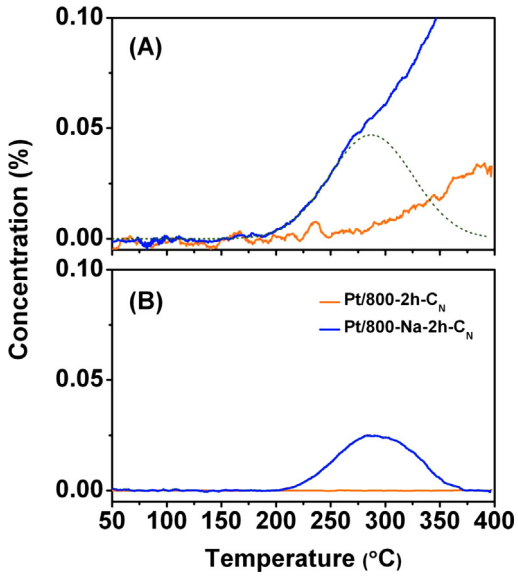

Fig. 10. CO-TPR of Pt/800-2h-C_N and Pt/800-Na-2h-C_N catalysts. (A) Carbon dioxide and (B) hydrogen evolution are shown. The green dotted line shows the deconvolution of the CO_2 contribution for the Na-promoted sample. Test conditions: 30 mL/min (10% CO–He); 10 °C/min; 0.1 g catalyst.

groups) on the support surface. By comparison, the activity Pt/Na-2h-C_N is unchanged over the course of reaction. In order verify the stability of these materials after the initial drop in the WGS activity of Pt/800-Na-2h-C_N, a long term stability test was performed as shown in Fig. 11. It is clear from these results that a minimal decrease in WGS activity is observed with time on stream under product-free conditions for both catalysts. This points to the stability of the Pt-Na-OH_x structures, even in the absence of surface oxygen groups. In a reformate-type gas feed containing hydrogen, however, the reaction rate over a Pt/800-Na-2h-C_N catalyst can be seen to decrease by ~2.5 times over the course of 24 h at 320 °C. The inhibitory effect of hydrogen on the WGS rate when using MWNT-based materials as well as the catalyst structural stability under reformate startup–shutdown conditions is under further investigation.

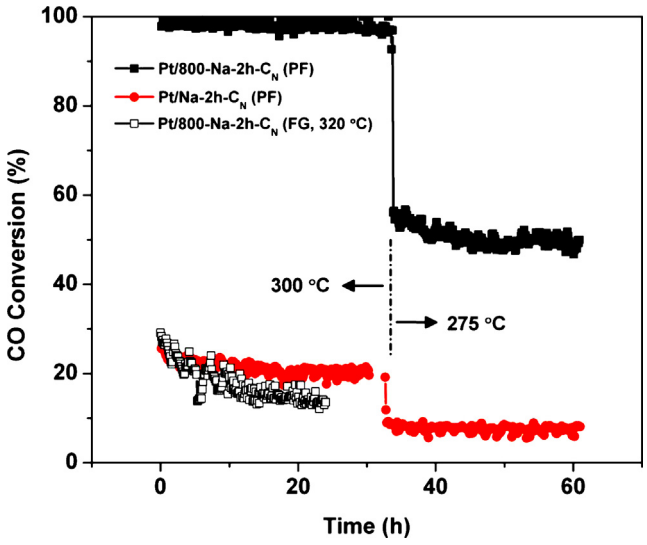

Fig. 11. WGS stability test of Na-promoted WGS catalysts under product-free (PF) and full reformate gas (FG) conditions. Gas flow rate = (PF) 70 mL/min (2% CO–10% H_2O–He) or (FG) 100 mL/min (11% CO–26%H_2–26%H_2O–7%CO_2–He); 0.1 g catalyst.

4. Conclusions

We have demonstrated, for the first time, a remarkable improvement in the activity of carbon-supported platinum for the WGS reaction by the controlled addition of a sodium promoter. It was found that oxidation of the MWNTs by nitric acid treatment prior to platinum addition results in a mild activation of the catalyst for WGS. The addition of sodium by ion-exchange alters the surface oxygen distribution significantly and substantially increases activity. Annealing the Na-exchanged MWNTs to 800 °C in He, although it drastically reduces the oxygen content, does not affect the ability of the surface to carry the Na-promoted Pt active sites for the WGS reaction and increases the number of these sites. Evidence for a previously proposed structure of alkali-promoted Pt-$(OH)_x$ active species for the WGS reaction has been given in this work on non-oxide surfaces. The sodium and platinum are shown to be in partially oxidized states on the carbon supports.

Acknowledgments

We acknowledge the financial support of this work by the U.S. Department of Energy/Basic Energy Sciences (Grant No. DE-FG02-05ER15730) and from the NSF (CBET Grant No. 0828666). The XPS and TEM work was performed at the Center for Nanoscale Systems (CNS), a member of the National Nanotechnology Infrastructure Network (NNIN), which is supported by the National Science Foundation under NSF Award No. ECS-0335765. CNS is part of Harvard University.

Appendix A. Supplementary data

Supplementary data associated with this article can be found, in the online version, at http://dx.doi.org/10.1016/j.apcatb.2013.07.013.

References

[1] W. Ruettinger, O. Ilinich, R.J. Farrauto, Journal of Power Sources 118 (2003) 65.
[2] C. Ratnasamy, J.P. Wagner, Catalysis Reviews – Science and Engineering 51 (2009) 325.
[3] M. Flytzani-Stephanopoulos, B.C. Gates, Annual Review of Chemical and Biomolecular Engineering 3 (2012) 545.

[4] Q. Fu, H. Saltsburg, M. Flytzani-Slephanopoulos, Science 301 (2003) 935.
[5] W. Deng, M. Flytzani-Stephanopoulos, Angewandte Chemie International Edition 45 (2006) 2285.
[6] P. Panagiotopoulou, D.I. Kondarides, Catalysis Today 112 (2006) 49.
[7] O. Thinon, K. Rachedi, F. Diehl, P. Avenier, Y. Schuurman, Topics in Catalysis 52 (2009) 1940.
[8] L.C. Grabow, A.A. Gokhale, S.T. Evans, J.A. Dumesic, M. Mavrikakis, Journal of Physical Chemistry C 112 (2008) 4608.
[9] A.A. Phatak, N. Koryabkina, S. Rai, J.L. Ratts, W. Ruettinger, R.J. Farrauto, G.E. Blau, W.N. Delgass, F.H. Ribeiro, Catalysis Today 123 (2007) 224.
[10] D. Tibiletti, F. Meunier, A. Goguet, D. Reid, R. Burch, M. Boaro, M. Vicario, A. Trovarelli, Journal of Catalysis 244 (2006) 183.
[11] C.T. Campbell, C.H.F. Peden, Science 309 (2005) 713.
[12] J.B. Park, J. Graciani, J. Evans, D. Stacchiola, S.D. Senanayake, L. Barrio, P. Liu, J.F. Sanz, J. Hrbek, J.A. Rodriguez, Journal of the American Chemical Society 132 (2010) 356.
[13] R. Si, M. Flytzani-Stephanopoulos, Angewandte Chemie International Edition 47 (2008) 2884.
[14] Y. Nagai, T. Hirabayashi, K. Dohmae, N. Takagi, T. Minami, H. Shinjoh, S. Matsumoto, Journal of Catalysis 242 (2006) 7.
[15] B. Qiao, A. Wang, X. Yang, L.F. Allard, Z. Jiang, Y. Cui, J. Liu, J. Li, T. Zhang, Nature Chemistry 3 (2011) 634.
[16] M. Hatanaka, N. Takahashi, T. Tanabe, Y. Nagai, K. Dohmae, Y. Aoki, T. Yoshida, H. Shinjoh, Applied Catalysis B 99 (2010) 336.
[17] W. Ruettinger, X. Liu, R.J. Farrauto, Applied Catalysis B 65 (2006) 135.
[18] X. Liu, W. Ruettinger, X. Xu, R. Farrauto, Applied Catalysis B 56 (2005) 69.
[19] R.J. Gorte, S. Zhao, Catalysis Today 104 (2005) 18.
[20] J.M. Pigos, C.J. Brooks, G. Jacobs, B.H. Davis, Applied Catalysis A 328 (2007) 14.
[21] H. Xie, J. Lu, M. Shekhar, J.W. Elam, W.N. Delgass, F.H. Ribeiro, E. Weitz, K.R. Poeppelmeier, ACS Catalysis 3 (2013) 61.
[22] H.N. Evin, G. Jacobs, J. Ruiz-Martinez, G.A. Thomas, B.H. Davis, Catalysis Letters 120 (2007) 166.
[23] G. Jacobs, B.H. Davis, International Journal of Hydrogen Energy 35 (2010) 3522.
[24] P. Panagiotopoulou, D.I. Kondarides, Journal of Catalysis 267 (2009) 57.
[25] Y. Zhai, D. Pierre, R. Si, W. Deng, P. Ferrin, A.U. Nilekar, G. Peng, J.A. Herron, D.C. Bell, H. Saltsburg, M. Mavrikakis, M. Flytzani-Stephanopoulos, Science 329 (2010) 1633.
[26] J.H. Pazmiño, M. Shekhar, W.D. Williams, M.C. Akatay, J.T. Miller, W.N. Delgass, F.H. Ribeiro, Journal of Catalysis 286 (2012) 279.
[27] Y. Wang, Y. Zhai, D. Pierre, M. Flytzani-Stephanopoulos, Applied Catalysis B 127 (2012) 342.
[28] D. Pierre, W. Deng, M. Flytzani-Stephanopoulos, Topics in Catalysis 46 (2007) 363.
[29] M.C. Román-Martínez, D. Cazorla-Amorós, A. Linares-Solano, C. de Lecea, Applied Catalysis A 116 (1994) 187.
[30] M. Toebes, Y. Zhang, J. Hajek, T. Nijhuis, J. Bitter, A. van Dillen, D. Murzin, D. Koningsberger, K. de Jong, Journal of Catalysis 226 (2004) 215.
[31] F.A. de Bruijn, V.A.T. Dam, G.J.M. Janssen, Fuel Cells 8 (2008) 3.
[32] S. Zhang, X.Z. Yuan, J.N.C. Hin, H. Wang, K.A. Friedrich, M. Schulze, Journal of Power Sources 194 (2009) 588.
[33] P. Hou, C. Liu, H. Cheng, Carbon 46 (2008) 2003.
[34] J.L. Figueiredo, M.F.R. Pereira, Catalysis Today 150 (2009) 2.
[35] D. Rosenthal, M. Ruta, R. Schlogl, L. Kiwi-Minsker, Carbon 48 (2010) 9.
[36] S. Kundu, Y. Wang, W. Xia, M. Muhler, Journal of Physical Chemistry C 112 (2008) 16869.
[37] H.P. Boehm, Carbon 40 (2001) 145.
[38] S. Haydar, C. Moreno-Castilla, M.A. Ferro-Garcia, F. Carrasco-Marin, J. Rivera-Utrilla, A. Perrard, J.P. Joly, Carbon 38 (2000) 1297.
[39] A. Linares-Solano, C. Salinas-Martínez de Lecea, D. Cazorla-Amorós, J.P. Joly, H. Charcosset, Energy and Fuels 4 (1990) 467.
[40] D. Cazorla-Amorós, A. Linares-Solano, C. Salinas-Martínez de Lecea, M. Nomura, H. Yamashita, A. Tomita, Energy and Fuels 7 (1993) 625.
[41] M.L. Toebes, J.M.P. van Heeswijk, J.H. Bitter, A. Jos van Dillen, K.P. de Jong, Carbon 42 (2004) 307.
[42] J.-W. Kim, H.-G. Lee, Metallurgical and Materials Transactions B 32 (2001) 17.
[43] E. Raymundo-Pinero, P. Azais, T. Cacciaguerra, D. Cazorla-Amorós, A. Linares-Solano, F. Beguin, Carbon 43 (2005) 10.
[44] L. Joncourt, M. Mermoux, P.H. Touzain, Journal of Physics and Chemistry of Solids 57 (1996) 877.
[45] R. Schlögl, H.P. Boehm, Carbon 22 (1984) 351.
[46] V.Z. Mordkovich, M. Baxendale, R.P.H. Chang, S. Yoshimura, Synthetic Metals 86 (1997) 2049.
[47] G. Fisher, B. Sexton, Physical Review Letters 44 (1980) 683.
[48] C.D. Wagner, D.A. Zatko, R.H. Raymond, Analytical Chemistry 52 (1980) 1445.
[49] J.-H. Zhou, Z.-J. Sui, J. Zhu, P. Li, D. Chen, Y.-C. Dai, W.-K. Yuan, Carbon 45 (2007) 785.
[50] A.J. Plomp, T. Schubert, U. Storr, K.P. de Jong, J.H. Bitter, Topics in Catalysis 52 (2009) 424.
[51] X. Wang, N. Li, J.A. Webb, L.D. Pfefferle, G.L. Haller, Applied Catalysis B 101 (2010) 21.
[52] V. Jiménez, A. Ramírez-Lucas, P. Sánchez, J.L. Valverde, A. Romero, International Journal of Hydrogen Energy 37 (2012) 4144.
[53] C. Matranga, B. Bockrath, Journal of Physical Chemistry B 109 (2005) 4853.
[54] Y. Shao, G. Yin, J. Wang, Y. Gao, P. Shi, Journal of Power Sources 161 (2006) 47.
[55] X. Hao, S. Barnes, J.R. Regalbuto, Journal of Catalysis 279 (2011) 48.
[56] M.A. Fraga, E. Jordao, M.J. Mendes, M.M.A. Freitas, J.L. Faria, J.L. Figueiredo, Journal of Catalysis 209 (2002) 10.
[57] A. Sepulveda-Escribano, F. Coloma, F. Rodríguez-Reinoso, Applied Catalysis A 173 (1998) 247.
[58] D.M. Zirl, S.H. Garofalini, Journal of Non-Crystalline Solids 122 (1990) 111.
[59] R. Caracciolo, S.H. Garofalini, Journal of the American Ceramic Society 71 (1988).
[60] M. Peuckert, H.P. Bonzel, Surface Science 145 (1984) 239.
[61] G. Fisher, J.L. Gland, Surface Science 94 (1980) 446.
[62] G.B. Fisher, B.A. Sexton, Physical Review Letters 44 (1980) 683.
[63] M. Ruckh, D. Schmid, M. Kaiser, R. Schaffler, T. Walter, H. Schock, Solar Energy Materials and Solar Cells 41–42 (1996) 335.
[64] R. Würz, M. Rusu, T. Schedel-Niedrig, M.C. Lux-Steiner, H. Bluhm, M. Hävecker, E. Kleimenov, A. Knop-Gericke, R. Schlögl, Surface Science 580 (2005) 80.
[65] H. Estrade-szwarckopf, B. Rousseau, C. Herold, P. Lagrange, Molecular Crystals and Liquid Crystals 310 (1998) 231.